Table 8. *Shortest intermolecular distances* (Å) *between non-hydrogen atoms*

O(4)–C(13)	2/011*	3·439 (6)	C(13)–O(6)	3/000	3·433 (6)
C(9)–C(15)	2/010	3·572 (5)	C(12)–C(15)	4/010	3·663 (6)
C(9)–C(14)	2/011	3·656 (6)	C(6)–O(4)	2/010	3·442 (5)
C(10)–C(15)	2/010	3·779 (5)	C(2)–O(2)	2/010	3·525 (5)
C(1)–O(3)	3/010	3·465 (5)	C(14)–C(9)	2/010	3·656 (6)
C(11)–O(4)	2/010	3·605 (5)	C(17)–O(3)	2/011	3·430 (7)

* Equivalent-position nomenclature: O(4)–C(13) 2/011 means O(4) at equivalent position (1) to C(13) at equivalent position (2), translated 0,1,1 unit cells in the **a**, **b** and **c** directions respectively. Code: (1) x,y,z; (2) $\frac{1}{2}-x,-y,\frac{1}{2}+z$; (3) $\frac{1}{2}+x,\frac{1}{2}-y,-z$; (4) $-x,\frac{1}{2}+y,\frac{1}{2}-z$.

Molecular packing

Fig. 3 illustrates the packing of the molecules in the plane (011). As shown in Table 8, no intermolecular distances are less than the sum of the van der Waals radii of the atoms involved, except that between C(9) and C(15).

The packing of the molecules can be described in terms of layers almost parallel to the *ab* plane (see equation of the mean plane of the rings). As shown in Fig. 3 and Table 8, each molecule is bound by van der Waals forces to six neighbouring molecules belonging to other layers.

This work was supported in part by CNRS (ERA No. 465, Dynamique des Cristaux Moléculaires) and by INSERM (U42).

References

BRISSE, F., JUST, G. & BLANK, F. (1978). *Acta Cryst.* B**34**, 557–562.

BUSING, W. R. & LEVY, H. A. (1964). *Acta Cryst.* **17**, 142–146.

GERMAIN, G., MAIN, P. & WOOLFSON, M. M. (1971). *Acta Cryst.* A**27**, 368–376.

HANSON, M. P., HERMAN, F., LEA, J. D. & SKILLMAN, S. (1964). *Acta Cryst.* **17**, 1040–1044.

MOULE, Y., JEMMALI, M. & ROUSSEAU, N. (1976). *Chem. Biol. Interactions*, **14**, 207–216.

MOULE, Y., MOREAU, S. & BOUSQUET, J. F. (1977). *Chem. Biol. Interactions*, **17**, 185–192.

RICHE, C., PASCARD-BILLY, C., DEVYS, M., GAUDEMER, A., BARBIER, M. & BOUSQUET, J. F. (1974). *Tetrahedron Lett.* pp. 2765–2766.

SCHOMAKER, V. & TRUEBLOOD, K. N. (1968). *Acta Cryst.* B**24**, 63–76.

STEWART, R. F., DAVIDSON, E. R. & SIMPSON, W. T. (1965). *J. Chem. Phys.* **42**, 3175–3187.

WEI, R. D., SCHNOES, H. K., HART, P. A. & STRONG, F. H. (1975). *Tetrahedron*, **31**, 109–114.

Acta Cryst. (1980). B**36**, 406–415

An X-ray Determination of the Charge Deformation Density in 2-Cyanoguanidine

BY F. L. HIRSHFELD

Department of Structural Chemistry, Weizmann Institute of Science, Rehovot, Israel

AND H. HOPE

Department of Chemistry, University of California, Davis, California, USA

(*Received* 31 *July* 1979; *accepted* 31 *October* 1979)

Abstract

The static deformation density of 2-cyanoguanidine has been mapped by least-squares refinement against low-temperature X-ray data extending to 2·77 $Å^{-1}$ in $2\sin\theta/\lambda$. Measured intensities were corrected empirically for extinction and scan truncation. The H atom vibration parameters were fixed with the aid of spectroscopic data. A multipole expansion of the deformation density imposed little more than minimum molecular symmetry and a nuclear cusp constraint. Qualitative and quantitative, *via* atomic partitioning, examination of the experimental deformation density supports the main predictions of simple resonance theory but shows better detailed agreement with SCF calculations on related molecules, including formamide and cyanogen azide. It also confirms the expected bond bending near the apex N atom.

Introduction

The structure of 2-cyanoguanidine, also called dicyandiamide, has long attracted the attention of crystallographers, who have applied both X-ray (Hughes, 1940; Zvonkova, Krivnov & Khvatkina, 1964) and

0567-7408/80/020406-10$01.00

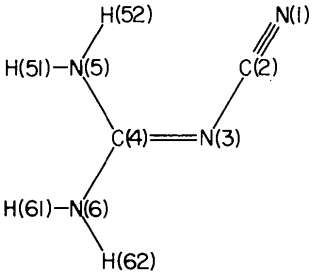

Fig. 1. Structural formula of 2-cyanoguanidine, showing atomic numbering and canonical valence-bond formula.

neutron diffraction (Rannev & Ozerov, 1964; Rannev, Ozerov, Datt & Kshnyakina, 1966) to its determination. Our interest in its electron distribution arises from several considerations. It combines in a small molecule a number of groups with distinctive electronic properties, notably the highly electronegative cyano group and the electron-donating amine group, whose electronic structures are of great chemical interest. Second, the standard structural formula (Fig. 1) patently fails to depict adequately the actual bonding pattern, as evidenced by the near equality of the three C–N lengths around C(4) (Hughes, 1940). An experimental map of the electron density cannot but throw light on the true valence structure of this molecule. Third, the observed (Rannev *et al.*, 1966) non-linearity of the N(3)–C(2)–N(1) arm and the inequality of the angles N(3)–C(4)–N(5) and N(3)–C(4)–N(6) both conform to a general pattern of tilted symmetric groups in analogous situations that has been ascribed (Hirshfeld, 1964) to a bending of the adjacent bonds. The observed deformation density in these bonds can provide a direct verification of this model.

Accordingly, a low-temperature X-ray study of cyanoguanidine was undertaken with the primary objective of mapping its static deformation density by least-squares refinement methods.

Data collection

To achieve the desired high resolution, necessary for establishing reliable vibration parameters, without scanning thousands of barely detectable high-order reflections, a two-stage strategy of data collection was adopted (Harel & Hirshfeld, 1975; Stevens & Hope, 1975, 1977; Hope & Ottersen, 1978). In the first stage all reflections out to S (= 2 sin θ/λ) = 1·3 Å^{-1} were measured. Their intensities were used for a low-resolution structure refinement with the standard free-atom model. Calculated structure factors from this low-order structure then permitted a simulation of the high-order intensity measurements, which served to identify those reflections beyond 1·3 Å^{-1} that could be measured with satisfactory precision. Measurement of these selected high-order reflections constituted the second stage of data collection.

Experimental

Colorless rectangular crystals of cyanoguanidine were grown by slow evaporation of an aqueous solution. X-ray diffraction showed monoclinic symmetry and the systematic absences (hkl with $h + k$ odd, $h0l$ with l odd) expected for space group $C2/c$ (Hughes, 1940).

A first set of intensities was measured at room temperature (Hope & Kim, 1971) but the present results have been obtained from a crystal held at about 83 K. All X-ray measurements were performed on an automated Picker diffractometer at the University of California, Davis. Graphite-monochromatized Mo $K\alpha$ radiation was used, with a crystal 0·35 × 0·35 × 0·35 mm. Cooling was provided by an Enraf–Nonius gas-flow device (van Bolhuis, 1971), modified for improved stability, better frost prevention, and lower consumption of liquid nitrogen. Long-term temperature variations were within ±0·1 K.

Intensities were measured in the $\theta/2\theta$ scan mode, at a rate d(2θ)/dt = 2° min^{-1}, over a range from $2\theta(\alpha_1)$ − 0·6° to $2\theta(\alpha_2)$ + 0·6°. Background intensity was interpolated linearly from stationary counts of 20 s at each end of the scan. Horizontal and vertical detector apertures were 1·35 and 1·47°, respectively. Attenuator foils kept the count rate below 9500 s^{-1}. A single strong reflection was monitored at intervals of 150 scans.

Low-temperature cell dimensions, obtained by least squares from the diffractometer setting angles of twelve Mo $K\alpha_1$ (λ = 0·70926 Å) reflections in the range 50 < θ < 60°, were: a = 14·8787 (16), b = 4·4238 (5), c = 13·0892 (12) Å, β = 115·63 (1)°. Corresponding values at 297 K were: a = 14·9712 (18), b = 4·4918 (6), c = 13·1062 (11) Å, β = 115·38 (1)°.

The low-order (S < 1·3 Å^{-1}) data comprised just over 800 independent reflections. After refinement of the structure described by Hughes (1940) against these data, a further 3200 reflections out to 2·77 Å^{-1} were selected, having a predicted relative precision $I/\sigma(I)$ > 15 for the indicated scan parameters. These brought the number N of measured reflections to 4002. The variances of the measured intensities I_o were tentatively estimated from Poisson statistics plus a term $(0{\cdot}005I_o)^2$ derived from the observed variance of the monitor intensities. Correction for absorption was found unnecessary. Approximate corrections for extinction and for scan truncation are described below.

Refinement

A preliminary refinement against the full data set used the spherical free-atom scattering factors except that H atoms were contracted to an effective nuclear charge $\zeta = 1{\cdot}2$. All atoms had anisotropic vibration parameters. In the course of this refinement the intensities were adjusted by an isotropic extinction correction, which replaced the input values of F_o by $F_{cor} = F_o/(1 - cF_o^2)$. The parameter c, adjusted repeatedly as the refinement proceeded, had a value close to $1{\cdot}2 \times 10^{-7}$, which increased the largest F_o by about 20%. The weights $w = 1/\sigma^2(F^2)$ were slightly reduced for the strongest reflections to allow for the uncertainty in the extinction correction. The free-atom refinement had $p = 92$ adjustable parameters, including the extinction coefficient c, and gave

$$R = \sum(F_o - kF_c)/\sum F_o = 0{\cdot}032;$$
$$r = [\sum w(F_o^2 - k^2F_c^2)^2/\sum wF_o^4]^{1/2} = 0{\cdot}090;$$
$$d = [\sum w(F_o^2 - k^2F_c^2)^2/(N-p)]^{1/2} = 5{\cdot}85.$$

Hydrogen parameters

In preparation for the deformation refinement it was necessary to specify a model for constraining the H atom vibration parameters (Hirshfeld, 1976). For this purpose approximate intramolecular force constants were transferred from formamide and *N*-methylacetamide (Miyazawa, Shimanouchi & Mizushima, 1958; Suzuki, 1960; Itoh & Shimanouchi, 1972). These led to estimated mean-square displacements of 0·005, 0·015 and 0·027 Å^2, respectively, for N–H bond stretching, in-plane bending, and out-of-plane bending. These internal vibrations were added to the rigid-body motion of the molecular skeleton, which was derived from a constrained refinement in which the five heavy atoms excluding N(1) were treated as a rigid unit. This RBM refinement, with 50 parameters, gave $R = 0{\cdot}033$, $r = 0{\cdot}099$, $d = 6{\cdot}39$. The H atom coordinates also were at first constrained by the assumption that the two NH_2 groups had identical dimensions and that each was symmetric about a twofold axis coincident with its C–N bond. Accordingly, the positions of the four H atoms were determined by four coordinates: the N–H length, the C–N–H angle, and the torsion angle of each NH_2 plane about the C–N bond axis. These constraints on the H atom positions and vibrational motions reduced the number of parameters for the free-atom model to 60 and led to $R = 0{\cdot}033$, $r = 0{\cdot}096$, $d = 6{\cdot}27$.

Deformation model

The deformation refinement retained the usual convolution approximation (Coulson & Thomas, 1971; Stewart, 1976), dividing the total charge density into atomic fragments that were assumed to undergo rigid harmonic translational vibrations only. Each of these pseudoatoms was treated as the sum of the static free-atom density and a deformation term; the latter was expanded in a basis of atomic multipole functions (Hirshfeld, 1971, 1977*c*)

$$\rho_{a,n,k}(\mathbf{r}) = N_n r_a^n \exp(-\alpha_a r_a)\cos^n\theta_{a,k}, \qquad (1)$$

where r_a is the distance from atomic center a, $\theta_{a,k}$ is the angle between the vector $\mathbf{r}_a$ and a specified axis $\mathbf{k}$ through the atomic center, α_a is an adjustable shape parameter for each atom, n is an integer between 0 and 4, and N_n is a normalizing factor proportional to α_a^{n+3}. Up to 35 deformation functions of this general form may be centered on each atom, corresponding to the different orders n and to different orientations of the polar axis $\mathbf{k}$, but the actual number of independent deformation coefficients $c_{a,n,k}$ was initially much smaller than this by virtue of several constraints that were imposed on the model (some of which were later relaxed – see below). Thus the cusp ($n = 0$) functions on C and N atoms were at first omitted, as were the fifteen fourth-order functions on H. The amine N(5) and N(6) atoms were assigned identical deformations, in correspondingly oriented axial frames, and the four H atoms were similarly made identical. C(2), N(3), and C(4) were assigned mirror symmetry with respect to local approximations to the mean molecular plane, while N(1), N(5), and N(6) were constrained to *mm* symmetry, the second mirror plane passing through the appropriate C–N bond in each case. For H atoms, full axial symmetry about the N–H bond was assumed. These constraints reduced the number of independent deformation parameters, including the exponential factors α_a, to 101: 22 each for C(2), N(3) and C(4), 14 each for N(1) and for the pair N(5) and N(6), and 7 for H atoms. Electric neutrality, maintained by the simple device (Harel & Hirshfeld, 1975) of assigning to F_{000} a value of 352 and a large statistical weight, lowered the effective number of deformation parameters to 100. Towards the end of this refinement the out-of-plane mean-square vibration amplitude of H atoms was allowed to vary, but it changed only from 0·027 to $0{\cdot}025 \pm 0{\cdot}003$ Å^2 (and was accordingly held at its original value in subsequent refinements). With a total of 161 refined parameters for this first deformation model $R = 0{\cdot}017$, $r = 0{\cdot}038$, $d = 2{\cdot}35$. The corresponding deformation density, of which a contour diagram in the molecular plane has been presented by Hirshfeld (1977*b*), already showed the essential features that were later confirmed by the further refinements described below.

Truncation correction

Throughout these early calculations a systematic discrepancy was evident in the high-angle reflections, where F_o was consistently smaller than F_c. The only

plausible explanation was the limited 2θ scan range, which causes truncation of the tails of the $K\alpha$ reflections together with an overestimate of the background intensity (Denne, 1977). Our correction for this twofold effect was derived from assumed Cauchy distributions for the α_1 and α_2 lines with half-widths of 0·00029 and 0·00032 Å, respectively (Compton & Allison, 1935). The actual scans extended 0·6° in 2θ on each side of the α_1–α_2 doublet (see above) but a much better fit was obtained on the assumption of a slightly narrower effective scan, from $2\theta(\alpha_1) - 0{\cdot}5°$ to $2\theta(\alpha_2) + 0{\cdot}5°$. This empirical adjustment may allow for unidentified instrumental factors, wavelength dependence of the scattering and detection efficiency, crystal misalignment, and the like. Very similar behavior has been found by Eisenstein (1979). The correction increased F_o by as much as 40% for the highest-angle reflections. At the same time the estimated variances of the corrected intensities were increased by the square of one-fourth of the correction. Refinement against the corrected data led to a small but systematic decrease in the vibration parameters, and gave $R = 0{\cdot}015$, $r = 0{\cdot}037$, $d = 1{\cdot}95$.

Final refinements

During the later refinement stages the RBM parameters, for evaluation of the H atom vibration parameters, were updated repeatedly *via* constrained refinements in which only the molecular **T**, **L**, and **S** tensors were adjusted. In these RBM refinements, N(1) was excluded from the rigid body because of apparent internal N–C≡N bending motion, while the H atoms were included with fixed excess mean-square amplitudes, including the out-of-plane component, as derived from their postulated internal vibrations.

Meanwhile, some of the more questionable constraints on the deformation model were relaxed. The symmetry of the deformation functions on N(5) and N(6), as well as on the H atoms, was lowered to *m*, leaving only N(1) with an additional local mirror plane through the C(2)–N(1) bond and perpendicular to the molecular plane. At the same time the cusp functions on all atoms were allowed non-zero coefficients. These changes raised the number of parameters to 180 and gave $R = 0{\cdot}015$, $r = 0{\cdot}035$, $d = 1{\cdot}89$. Such a modest improvement, brought about by the addition of the last 20 deformation parameters, suggested that no further increase in the flexibility of the deformation model was warranted. A contour map of the deformation density at this stage, and of its atomic fragments, has been presented by Eisenstein & Hirshfeld (1979).

Before the results could be accepted as final, several further modifications seemed to be required. Serious uncertainty was attached to the statistical weights of the low-angle reflections. These reflections appeared, on average, to suffer anomalously large discrepancies between F_o and F_c that no improvement in the deformation model thus far had succeeded in eliminating. The discrepancies did not appear to obey any systematic pattern and a difference Fourier synthesis showed mainly random noise. These indications implied that the intensity data in this region were less accurate than our initial error estimates had assumed. It thus became necessary to reduce the statistical weights of these reflections; accordingly the estimated variances $\sigma^2(F^2)$ were adjusted empirically by the addition of a term proportional to $(F_o/S^2)^2$. With this modification, the average values of $w[\Delta(F^2)]^2$ were nearly uniform in different ranges of F and of S. Refinement with the modified weights yielded $R = 0{\cdot}0149$, $r = 0{\cdot}0309$, $d = 1{\cdot}216$. However, this refinement tended to be unstable, showing a slow but persistent drift of the N–H length to unacceptably short values. The discrepancy indices quoted correspond to a local minimum or pseudominimum obtained with the N–H distance fixed at about 0·98 Å. [For comparison we also repeated, with the revised weights, the refinement of the more constrained model (100 deformation parameters) and obtained trouble-free convergence to $R = 0{\cdot}0147$, $r = 0{\cdot}0311$, $d = 1{\cdot}220$. This comparison confirms that the symmetry constraints imposed no severe limitation on the flexibility of the deformation model.]

The next change concerned the form of the cusp functions ($n = 0$; equation 1). If we neglect contributions to the deformation density at each nucleus from deformation functions centered on neighboring nuclei, the Kato nuclear cusp constraint (Bingel, 1963) requires the exponent α_a of the cusp function

$$\rho_{a,0}(\mathbf{r}) = N_0 \exp(-\alpha_a r_a)$$

on an atom of nuclear charge Z_a to have the value

$$\alpha_{a,0} = 2Z_a/a_o$$

(Eisenstein, 1979), where a_o is the Bohr radius 0·5292 Å. Application of this cusp constraint required distinguishing between two exponents for each atom type: the fixed exponent $\alpha_{a,0}$ defined above for the cusp function alone and the variable parameter α_a for all other deformation functions on the atom. It was not expected that the X-ray data would be sensitive to this modification of the cusp behavior close to the atomic nuclei. Indeed, the results were inappreciably affected except that convergence was entirely smooth. Refinement yielded a very similar deformation map, except at the nuclear positions, and $R = 0{\cdot}0147$, $r = 0{\cdot}310$, $d = 1{\cdot}217$.

Finally, the structural model was relaxed by removal of the geometric constraints on the H atom positions. Refinement of independent H atom coordinates brought the number of parameters to 188 and led to a substantial improvement in the agreement between F_o and F_c, especially for the low-angle reflections. This

permitted a less drastic downweighting of the low-angle intensities than had previously seemed necessary. Also, the functional form of the extra variance term was changed to $(F_o/S)^2$, corresponding to a more gradual S dependence in the low-S region. Refinement with the altered weights converged smoothly to $R = 0{\cdot}0133$, $r = 0{\cdot}0296$, $d = 1{\cdot}096$.

Results

Structural data

Final coordinates and vibration parameters are listed in Tables 1 and 2. Bond lengths and angles are shown in Fig. 2. The corrected bond lengths are based on the riding model (Busing & Levy, 1964) for N(1)–C(2) and rigid-body libration for the other C–N bonds. The N–H distances have been corrected both for rigid-body libration and for the riding motion due to the postulated N–H-bending vibrations, the two corrections being applied additively. Displacements of atoms from the mean molecular plane are given in Table 3 and Fig. 2.*

In Table 4 the rigid-bond test (Hirshfeld, 1976) is applied to the vibration parameters of the non-hydrogen atoms. The r.m.s. discrepancy between C and N mean-square amplitudes along each C–N bond is 0·00013 Å^2, just over the average value of $2\sigma(u^2)$, compared with 0·00087 Å^2 for the free-atom model. The mean-square displacements are less than a third

Table 1. *Fractional atomic coordinates* ($\times 10^5$ *for* C, N; $\times 10^3$ *for* H)

E.s.d.'s are given in parentheses.

	x	y	z
N(1)	16673 (1)	−1017 (4)	−12464 (1)
C(2)	13306 (1)	10528 (5)	−6860 (2)
N(3)	9069 (1)	24773 (5)	−1365 (2)
C(4)	11530 (1)	16819 (4)	9408 (2)
N(5)	18352 (1)	−4259 (4)	15010 (2)
N(6)	7029 (1)	31346 (4)	14831 (2)
H(51)	192 (1)	−111 (3)	224 (2)
H(52)	217 (1)	−159 (4)	115 (2)
H(61)	85 (1)	260 (3)	227 (2)
H(62)	18 (1)	462 (4)	109 (2)

Table 2. *Atomic mean-square vibration amplitudes* (Å$^2 \times 10^5$)

E.s.d.'s are given in parentheses. Hydrogen values were not refined.

	U^{11}	U^{22}	U^{33}	U^{12}	U^{23}	U^{13}
N(1)	1551 (6)	1944 (8)	1080 (6)	118 (4)	−268 (4)	805 (5)
C(2)	1106 (6)	1372 (7)	768 (5)	90 (4)	−66 (4)	488 (4)
N(3)	1143 (5)	1352 (5)	741 (4)	288 (4)	88 (3)	456 (3)
C(4)	874 (4)	947 (5)	712 (4)	46 (3)	0 (3)	371 (3)
N(5)	1270 (5)	1188 (5)	972 (4)	358 (4)	225 (3)	557 (3)
N(6)	1270 (5)	1328 (5)	874 (4)	329 (4)	66 (3)	578 (3)
H(51)	3950	3594	1911	1287	1019	1621
H(52)	3661	3527	2711	1646	503	2050
H(61)	3338	3404	1545	763	465	1255
H(62)	3730	3888	2517	2301	985	1507

Table 3. *Atomic displacements* (Å) *from the mean molecular plane*

The indicated standard deviations apply to displacements from the fixed reference plane defined by $-9{\cdot}779787x - 3{\cdot}049615y + 0{\cdot}130639z + 1{\cdot}628863 = 0$. This plane contains the two smallest inertial axes of the molecule, as derived from the experimental atomic coordinates. The dependence of the coefficients in the above equation on these coordinates is not reflected in the e.s.d.'s.

N(1)	+0·0130 (2)	N(6)	+0·0049 (2)
C(2)	−0·0025 (2)	H(51)	+0·117 (16)
N(3)	−0·0153 (2)	H(52)	+0·010 (16)
C(4)	+0·0007 (2)	H(61)	+0·029 (15)
N(5)	−0·0165 (2)	H(62)	+0·061 (18)

* A list of structure factors has been deposited with the British Library Lending Division as Supplementary Publication No. SUP 34829 (13 pp.). Copies may be obtained through The Executive Secretary, International Union of Crystallography, 5 Abbey Square, Chester CH1 2HU, England.

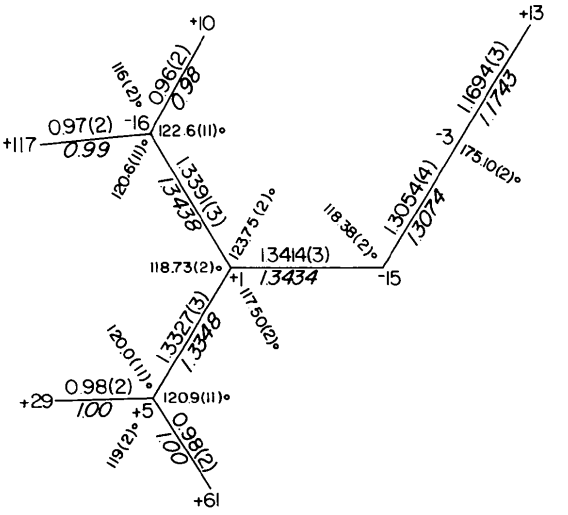

Fig. 2. Bond lengths (Å) and angles, with e.s.d.'s in parentheses. Vibration-corrected bond lengths in italics are based on the riding model for C(2)–N(1), rigid-body libration for other C–N bonds, libration plus riding motion for N–H bonds. Signed figures give atomic displacements from mean molecular plane (Å $\times 10^3$).

Table 4. *Mean-square vibration amplitudes* (Å$^2 \times 10^5$) *of bonded atoms A and B in the direction of bond A–B, for rigid-bond test of vibration parameters*

		Free-atom refinement		Deformation refinement	
A	*B*	$z^2_{A,B}$	$z^2_{B,A}$	$z^2_{A,B}$	$z^2_{B,A}$
N(1)	C(2)	928	941	764	755
C(2)	N(3)	978	819	791	808
N(3)	C(4)	752	807	726	713
C(4)	N(5)	958	899	861	850
C(4)	N(6)	840	766	753	765
R.m.s. discrepancy		87		13	

and their e.s.d.'s about a fifth of the corresponding quantities at room temperature, but the comparison between the spherical-atom and the deformation models closely parallels the results obtained at room temperature (Hirshfeld, 1976). We conclude that the deformation refinement has succeeded in distinguishing between the static deformation density and the effects of thermal smearing. This result supports the validity both of the convolution approximation and of our deformation expansion.

Deformation density

Fig. 3 presents a section, in the mean molecular plane, through the static deformation density of a single molecule. This has been extracted, as specified below, from the triply periodic deformation density of the entire crystal given by

$$\delta\rho(\mathbf{r}) = \sum_{a,n,k}{}' c_{a,n,k}\rho_{a,n,k}(\mathbf{r})$$

(see equation 1). Perpendicular sections through several bonds are shown in Fig. 4. The most conspicuous features of the deformation density are the expected bond and lone-pair maxima balanced by diffuse hollows in other directions around the several atoms. The e.s.d. $\sigma(\delta\rho)$ in the C—N bond peaks, obtained from the least-squares covariance matrix (Rees, 1977), is typically 0·03 to 0·04 e Å^{-3}. It has also been checked that the *total* density ρ is positive everywhere. The positions of the heavy atoms, left blank in Figs. 3 and 4, are marked by sharp peaks in both $\delta\rho$ and $\sigma(\delta\rho)$ (Table 5), which tell us essentially nothing about the actual deformation density at these positions. It is not just coincidence that the apparent values of $\delta\rho$ at these atomic centers are all positive though experimentally insignificant; the coefficients of the corresponding cusp functions are all strongly correlated (88 to 96%) with each other, being negatively correlated (−96 to −99%) with the scale factor k. The deformation density at the H atom nuclei is 0·91 ± 0·12 e Å^{-3} but the e.s.d. is probably unreliable because of the approximate treatment of the H atom vibrational motion.

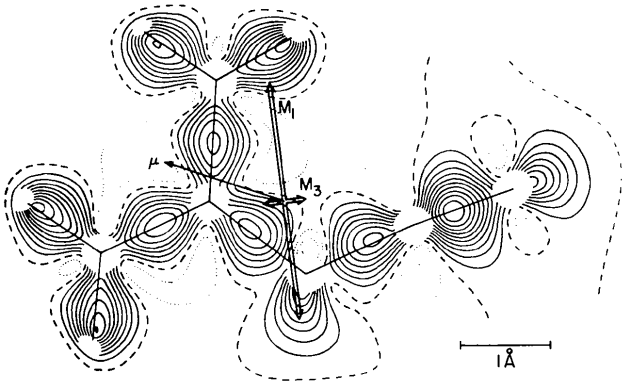

Fig. 3. Static molecular deformation density, partitioned from crystal density, in the mean molecular plane. Contour interval = 0·1 e Å^{-3}; the zero contour is indicated as a broken line and negative contours are dotted. Blank regions have $\sigma(\delta\rho) >$ 0·1 e Å^{-3}. Arrows through the center of gravity show directions of molecular dipole moment μ and principal second moments M_1 and M_3.

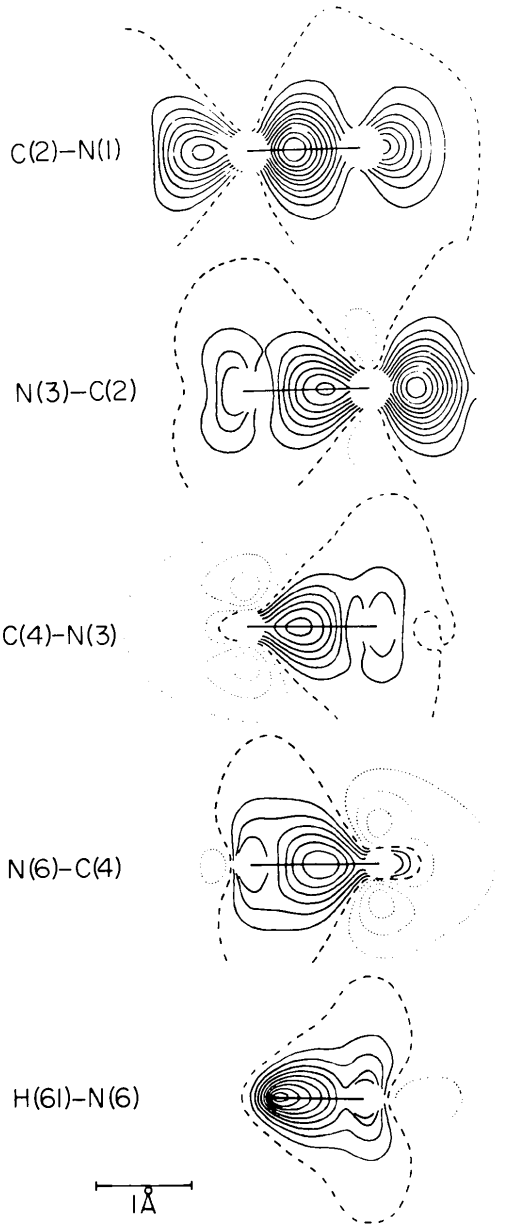

Fig. 4. The deformation density in sections through several bonds, perpendicular to mean molecular plane. Contours are as in Fig. 3. Omitted sections through C(4)–N(5) and three N–H bonds are virtually identical, respectively, to the C(4)–N(6) and N(6)–H(61) sections shown.

Table 5. *Deformation densities and their e.s.d.'s at the atomic centers* (e Å^{-3})

	$\delta\rho$	$\sigma(\delta\rho)$		$\delta\rho$	$\sigma(\delta\rho)$
N(1)	2	17	H(51)	0·91	0·12
C(2)	10	10	H(52)	0·91	0·12
N(3)	19	17	H(61)	0·90	0·12
C(4)	6	10	H(62)	0·91	0·12
N(5)	16	16			
N(6)	16	16			

Atomic partitioning

A more quantitative description of the molecular charge distribution may be obtained *via* an atomic decomposition of the observed deformation density. For this purpose the deformation density associated with a central molecule plus adjacent portions, up to an atom–atom separation of 5 Å, of 20 neighboring molecules, comprising a total of 115 atoms, was partitioned into atomic fragments according to the stockholder recipe of Hirshfeld (1977*a*). The fragments, so defined, belonging to the central molecule were then summed to produce the molecular deformation density, partitioned from its neighbors, and this is the function plotted in Figs. 3 and 4. The same atomic fragments served for the quantitative characterization of the deformation density *via* the atomic net charges and first and second moments. These were evaluated by numerical integration on an orthogonal 0·2 Å grid and the results, in a convenient local coordinate frame on each atomic center, are listed in Table 6. A calculated net charge imbalance of −0·019 e reflects the inaccuracy of the numerical integrations; this was estimated by displacing the grid origin by half its body diagonal and repeating the integrations. The values in Table 6 are the averages from the two interpenetrating grids.

Direct evaluation, from the least-squares covariance matrix, of the e.s.d.'s of the tabulated multipole components (Rees, 1977) would be cumbersome and not entirely reliable. We prefer to judge the likely accuracy of these quantities from the stability of the values obtained at successive stages of the refinement. In this way we find the net charges q to have e.s.d.'s about 0·08 e for C and N, and about 0·04 e for H. The dipole-moment components μ_i are probably accurate to within 0·03 to 0·06 e Å for the heavier atoms, and 0·02 to 0·05 e Å for H, the larger estimates pertaining to the longitudinal components μ_L of the cyano-group atoms and of H. For the second moments, μ_{ij}, the estimated errors are about 0·06 e Å^2 for C and N, and 0·04 e Å^2 for H. These error estimates, subjective as they are, discourage the assignment of much more than qualitative significance to most of the values in Table 6.

However, even a semi-quantitative interpretation of these data reveals several features in general accord with previous experience and chemical intuition. Among these is the expected overall charge migration from the two amine groups on to the highly electronegative cyano group. The H atoms show the typical pattern predicted by SCF calculations on small molecules (Hirshfeld, 1977*a*, 1979), *i.e.* a positive net charge of about 0·1 e, forward polarization into the bonds (negative μ_L), and roughly isotropic charge contraction (positive values of all three diagonal second moments μ_{ii}). The heavier atoms also show an overall charge contraction (mainly positive second moments) while the conspicuously large value of μ_{NN} on C(4) is primarily attributable to a loss of charge from its $2p_\pi$ orbital, largely to its negatively charged neighbor N(3). This loss is evident in the perpendicular sections through several C–N bonds (Fig. 4), which show a pair of deep troughs in the π regions of C(4), surrounded by positive peaks in the corresponding regions of its three ligands. In general the values of μ_{NN} on the heavy atoms correlate almost linearly with their net charges q, implying that much of the observed interatomic charge migration is concentrated in the π orbitals.

SCF calculations on several linear cyano compounds (Hirshfeld, 1977*a*) and on cyanogen azide (Hirshfeld,

Table 6. *Net charges q* (e × 10^2), *dipole moments* μ_i (e Å × 10^2), *and second moments* μ_{ij} (e Å^2 × 10^2) *of atomic fragments of deformation density, referred to local atomic axes* **L,M,N**

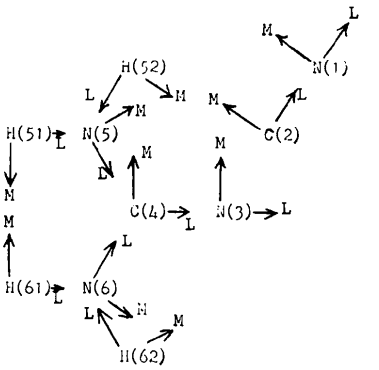

Second-moment components μ_{LN} and μ_{MN} nearly vanish by symmetry and are not listed.

	q	μ_L	μ_M	μ_{LL}	μ_{MM}	μ_{NN}	μ_{LM}
N(1)	−29	+2	+1	−2	+2	+2	−1
C(2)	+7	−8	+2	−2	+19	+18	+1
N(3)	−21	−3	+3	+4	+4	+5	0
C(4)	+22	−2	+1	+11	+11	+25	0
N(5)	−9	−2	0	+10	+10	+12	0
N(6)	−12	−3	−1	+9	+10	+10	0
H(51)	+11	−5	−2	+4	+7	+7	+1
H(52)	+10	−5	−1	+3	+6	+7	0
H(61)	+10	−5	−2	+3	+7	+7	+1
H(62)	+8	−4	−1	+2	+6	+7	0

1979) yield negative values for μ_L on the terminal N atom; a similar result was obtained from the present X-ray study at an earlier refinement stage (Hirshfeld, 1977*b*). These results imply that polarization of this atom into the lone-pair region outweighs the opposite polarization into the C≡N bond. The present data, with a slightly positive value for μ_L on N(1), seem to reverse this conclusion, but the result is far too uncertain to be meaningful. It also depends crucially on the way the deformation density has been partitioned between neighboring molecules.

The integrations summarized in Table 6 lead to an experimental molecular dipole moment $\mu = 1{\cdot}41$ e Å = $6{\cdot}76$D = $22{\cdot}6 \times 10^{-30}$ Cm in a direction 19° from the N(3)–C(4) bond vector (Fig. 3). The second moment of the molecular deformation density is positive definite, implying an overall charge contraction in all directions. Its principal values are $M_1 = 1{\cdot}66$, $M_2 = 1{\cdot}00$, $M_3 = 0{\cdot}30$ e Å^2, of which the largest and smallest lie nearly in the mean molecular plane (Fig. 3). The corresponding quadrupole moments are 4·86 and −4·96 Buckinghams in the plane and 0·10 Buckinghams in the normal direction (16·2, −16·5, and $0{\cdot}3 \times 10^{-40}$ Cm^2).

As suggested above, these outer moments of the deformation density, of the molecule as of the individual atoms, are highly sensitive to the way the total deformation density in the crystal has been allocated among these units. We have no assurance that our partitioning recipe gives the best approximation to the deformation density of an isolated molecule, even supposing the crystal deformation density to have been precisely determined. On the whole, the chosen recipe tends to produce minimum values for the outer moments of the molecular deformation density since it allows a mutual cancellation of overlapping positive and negative densities from expansion functions centered on neighboring molecules. If, for example, we simply sum the deformation functions centered on the atoms of one molecule, the dipole moment μ rises to 2·34 e Å and the principal second moments become $M_1 = 2{\cdot}26$, $M_2 = 0{\cdot}96$, $M_3 = 0{\cdot}16$ e Å^2. With such a summation, however, the total density has occasional negative excursions, though the deepest of these is only −0·003 e Å^{-3}.

Resonance interpretation

Hughes (1940) explained the nearly equal C–N lengths around C(4) (Fig. 2) by resonance, chiefly among the three structures (*a*)–(*c*).

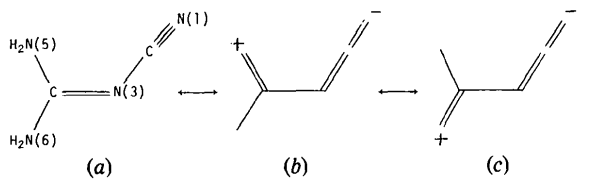

(*a*) (*b*) (*c*)

Such an interpretation leads directly to several specific predictions about the molecular deformation density that can be checked against the present results:

(1) We expect the net atomic charges to reflect the postulated partial negative charge on N(1) and positive charges on the amine groups. N(1) indeed carries a negative charge of 0·3 e, while each NH_2 group, taken as a whole, has a net positive charge of about 0·1 e (Table 6). However, the large negative charge of −0·2 e on N(3) suggests that the two additional resonance structures (*d*) and (*e*) may be nearly as important as (*b*) and (*c*) above.

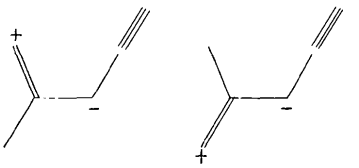

(*d*) (*e*)

(2) The perpendicular sections through the three bonds from C(4) to its ligand N atoms should show comparable π-bonding density in these three bonds. The highly diffuse character of the π density makes it difficult to verify this prediction with any confidence, but the appearance of the relevant sections (Fig. 4) seems consistent with our expectation. In fact, the C(4)–N(5) and C(4)–N(6) bond peaks are appreciably more extended in the out-of-plane direction than the C(4)–N(3) peak, implying that the charge-separated structures (*b*)–(*e*) together represent the true π-orbital distribution better than structure (*a*) alone.

(3) The predicted π bonding in the C(2)–N(3) bond should likewise be reflected in the perpendicular section through this bond. Direct comparison with the bonds around C(4) is not possible since C(2), with its linear hybridization, forms shorter and stronger σ bonds than does the trigonally hybridized C(4). Yet a qualitative comparison of the corresponding sections in Fig. 4 suggests that there is at least as much π density in the C(2)–N(3) bond as in C(4)–N(3), *i.e.* that structures (*b*) and (*c*) jointly contribute at least as much as (*a*) to the total valence structure.

(4) The cyano bond, N(1)–C(2), predicted by structures (*a*), (*d*), and (*e*) to be axially symmetric, should lose this symmetry by virtue of the allenic structures (*b*) and (*c*) and show greater in-plane than perpendicular π bonding. If the relative strengths of π bonding in the two planes can be judged from the shape of the 0·1 e Å^{-3} contour in Figs. 3 and 4, this prediction is not supported by the observed deformation density. The 0·1 contour is in fact noticeably broader in the perpendicular direction than in the molecular plane. In this respect the resonance picture is contradicted not only by our observed deformation density but also by *ab initio* calculations on model compounds (see below).

(5) The asymmetry due to structures (*b*) and (*c*) should show up also in the lone-pair density on N(1). This density should be elongated in the out-of-plane direction, in a manner analogous to the 'rabbit ear' lobes of a carbonyl O atom with its σ orbitals in the perpendicular plane. Comparison of Figs. 3 and 4 indeed shows the N(1) lone-pair peak to be appreciably more extended in the perpendicular section than in the molecular plane.

Comparisons with SCF theory

More precise and detailed comparisons can be made with the results of SCF calculations on related small molecules. For example, extended-basis calculations on formamide (Stevens, Rys & Coppens, 1978; Eisenstein, 1979) have produced nearly identical deformation density maps which are very similar in the NH_2 region to our experimental map of cyanoguanidine. The net atomic charges calculated by Eisenstein (Hirshfeld, 1979) are −0·14 e on N and +0·13 to 0·14 e on each H, in qualitative agreement with the present values of −0·09 and −0·12 e on N(5) and N(6), respectively, and +0·08 to +0·11 e on the H atoms (Table 6). The theoretical and experimental maps both show a nearly symmetric array of three bond peaks around the N atom separated by three narrow troughs of charge deficiency. Both show excess density above and below the N atom, merging with a C–N bond peak that is broadly extended in the out-of-plane direction but, in the molecular plane, is narrowly confined between large areas of moderate charge depletion.

The N(3)–C(2)–N(1) region of cyanoguanidine can be compared with the SCF deformation density of cyanogen azide (Fig. 5), likewise derived from an extended-basis wavefunction (Eisenstein & Hirshfeld, 1979). The theoretical net atomic charges (Hirshfeld, 1979) on the apex N atom and the cyano C and N atoms are, respectively, −0·13, +0·10, and −0·24 e, closely parallel to the cyanoguanidine values −0·21, +0·07, and −0·29 e (Table 6). Apart from the immediate vicinity of the atomic nuclei, the in-plane sections through the two molecular deformation densities show a closely similar pattern of peaks and valleys. This similarity extends even to the slight displacements of the C–N bond peaks off the internuclear axes, including the scarcely perceptible displacement of the large peak in the terminal C≡N bond. Of particular interest is the shape of this terminal-bond peak, which, in cyanogen azide as in cyanoguanidine, is predicted by simple resonance arguments to be intermediate between a double and a triple bond. Comparison of the in-plane and out-of-plane sections (Fig. 5) shows, as in cyanoguanidine (Figs. 3, 4), no evidence of the expected asymmetry of this peak. On the other hand the lone-pair peak behind the terminal N atom is, as predicted, definitely broader in the perpendicular than in the in-plane direction. The calculated deformation density in cyanogen azide thus agrees in all essential respects with the observed density in cyanoguanidine.

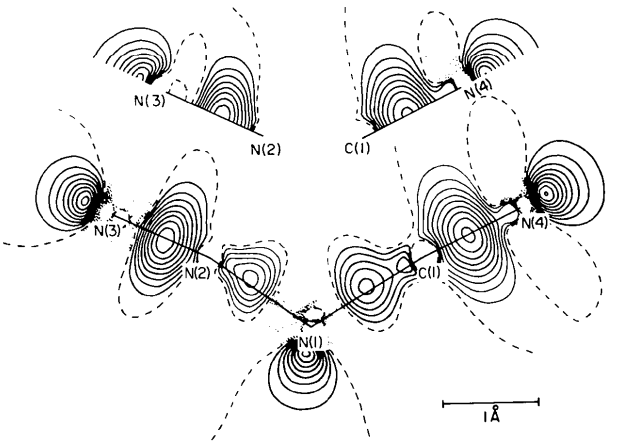

Fig. 5. SCF deformation density of cyanogen azide in the molecular plane and in perpendicular sections through the two terminal bonds. Contours as in Fig. 3 (Eisenstein & Hirshfeld, 1979).

A formally analogous situation occurs in the azido arm of the cyanogen azide molecule as well as in hydrazoic acid, HN_3. In both instances resonance arguments imply that the terminal N≡N linkage should include a full π bond in the molecular plane but only a partial π bond in the perpendicular plane. Again, the SCF deformation densities (Eisenstein & Hirshfeld, 1979; Hirshfeld, 1979) fail to bear out the expected asymmetry of the N≡N bond peak but do confirm the related expectation that the lone-pair densities on the terminal N atoms in these two molecules should be broader in the out-of-plane direction than in the molecular plane.

Accordingly, the consistent verdict of our experimental deformation map of cyanoguanidine and of SCF calculations on hydrazoic acid and cyanogen azide is that simple resonance arguments correctly predict the shape of the lone-pair density on all four terminal N atoms in these three molecules but not that of the adjacent bond peaks.

It may be unfair to expect resonance theory to predict the shape of the π-bonding density, inasmuch as no molecular symmetry justifies the distinction between σ and in-plane π orbitals. Rather, hybridization of the π bonding orbital with an antibonding σ orbital may yield an apparent contraction of the density in this region towards the bond axis. Such mixing of σ and π orbitals must also be responsible for the lateral displacement of the density peak off the C–N axis, which we find in both cyanoguanidine (Fig. 3) and cyanogen azide (Fig. 5).

Similar reasoning evidently accounts for the slight rotation of the lone-pair peaks behind both terminal N atoms in cyanogen azide to positions *trans* with respect to the apex N atom (Fig. 5). Each of these peaks is, on

this argument, displaced by hybridization with a locally antibonding π orbital largely localized in the region of the adjacent bond. The effect would thus be analogous to the preference of ethylene for the *anti* rather than the *syn* mode of pyramidalization (Volland, Davidson & Borden, 1979) and to the similarly favored *trans* mode of bending in acetylene (Strozier, Caramella & Houk, 1979). This explanation is supported by the computational finding that the similar off-axis displacement of the N atom lone-pair peak in hydrazoic acid vanishes when the azido chain is made linear (Eisenstein & Hirshfeld, 1979). In the same way, Eisenstein (unpublished calculations) has found that when HCN is bent the N atom lone-pair peak moves to a position *trans* with respect to the H atom. In all cases the terminal N atom appears simply to rotate in the plane, turning its σ bonding orbital to one side of the bond axis and its lone-pair orbital to the opposite side. This is best seen in Fig. 3(*c*) of Eisenstein & Hirshfeld (1979), where the SCF deformation density of hydrazoic acid is partitioned into its atomic components. In cyanoguanidine, Fig. 3 clearly shows the small downward displacement of the C≡N bond peak while the predicted upward shift of the lone-pair peak might perhaps have been discernible but for our imposition of *mm* symmetry on the N atom deformation functions.

Bent bonds

A major reason for our interest in the deformation density of cyanoguanidine was the hope of verifying a predicted bending of the two bonds to N(3). At the other end of each of these C–N bonds lies a symmetric ligand, a cyano group at one end of the molecule and a diaminomethylene fragment at the other, and each of these has its symmetry axis tilted away from the direction of the bond joining it to N(3). The cyano bond C(2)–N(1) is turned 5° from collinearity with N(3)–C(2) while the angles around C(4) show the bisector of angle N(5)–C(4)–N(6) to be inclined 3° from the direction of the bond C(4)–N(3) (Fig. 2). Both these deviations may be simply explained (Hirshfeld, 1964) as direct consequences of a bending of the N(3)–C(2) and N(3)–C(4) bonds by strong repulsion between C(2) and C(4) at a non-bonded separation of 2·273 Å. Such bending should be directly observable in an accurate deformation density map. As expected, Fig. 3 shows these two bond peaks to be conspicuously displaced off the straight internuclear lines in the predicted directions, by 0·04 Å for N(3)–C(2) and by 0·025 Å for N(3)–C(4). This bent-bond model has been shown (Eisenstein & Hirshfeld, 1979) to have quite general validity, accounting for off-axis bond peaks in SCF deformation maps of several small molecules, including hydrazoic acid and cyanogen azide discussed above. In these two molecules the predicted bond bending is associated with slightly non-linear valence angles analogous to that found at C(2) in cyanoguanidine.

This research was supported by grants from the United States National Science Foundation and from the United States–Israel Binational Science Foundation (BSF), Jerusalem, Israel.

References

BINGEL, W. A. (1963). *Z. Naturforsch. Teil A*, **18**, 1249–1253.

BOLHUIS, F. VAN (1971). *J. Appl. Cryst.* **4**, 263–264.

BUSING, W. R. & LEVY, H. A. (1964). *Acta Cryst.* **17**, 142–146.

COMPTON, H. C. & ALLISON, S. K. (1935). *X-rays in Theory and Experiment*. New York: Van Nostrand.

COULSON, C. A. & THOMAS, M. W. (1971). *Acta Cryst.* B**27**, 1354–1359.

DENNE, W. A. (1977). *Acta Cryst.* A**33**, 438–440.

EISENSTEIN, M. (1979). *Acta Cryst.* B**35**, 2614–2625.

EISENSTEIN, M. & HIRSHFELD, F. L. (1979). *Chem. Phys.* **38**, 1–10; **42**, 465–474.

HAREL, M. & HIRSHFELD, F. L. (1975). *Acta Cryst.* B**31**, 162–172.

HIRSHFELD, F. L. (1964). *Isr. J. Chem.* **2**, 87–90.

HIRSHFELD, F. L. (1971). *Acta Cryst.* B**27**, 769–781.

HIRSHFELD, F. L. (1976). *Acta Cryst.* A**32**, 239–244.

HIRSHFELD, F. L. (1977*a*). *Theor. Chim. Acta*, **44**, 129–138.

HIRSHFELD, F. L. (1977*b*). *Isr. J. Chem.* **16**, 198–201.

HIRSHFELD, F. L. (1977*c*). *Isr. J. Chem.* **16**, 226–229.

HIRSHFELD, F. L. (1979). *Proceedings of NATO Advanced Study Institute on Electronic and Magnetic Distributions in Molecules and Crystals, Arles*, pp. 757–768. New York: Plenum.

HOPE, H. & KIM, N. E. (1971). Am. Crystallogr. Assoc. Winter Meet., Abstr. p. 22.

HOPE, H. & OTTERSEN, T. (1978). *Acta Cryst.* B**34**, 3623–3626.

HUGHES, E. W. (1940). *J. Am. Chem. Soc.* **62**, 1258–1267.

ITOH, K. & SHIMANOUCHI, T. (1972). *J. Mol. Spectrosc.* **42**, 86–99.

MIYAZAWA, T., SHIMANOUCHI, T. & MIZUSHIMA, S. (1958). *J. Chem. Phys.* **29**, 611–616.

RANNEV, N. V. & OZEROV, R. P. (1964). *Dokl. Phys. Chem.* **155**, 426–428.

RANNEV, N. V., OZEROV, R. P., DATT, I. D. & KSHNYAKINA, A. N. (1966). *Sov. Phys. Crystallogr.* **11**, 177–181.

REES, B. (1977). *Isr. J. Chem.* **16**, 180–186.

STEVENS, E. D. & HOPE, H. (1975). *Acta Cryst.* A**31**, 494–498.

STEVENS, E. D. & HOPE, H. (1977). *Acta Cryst.* A**33**, 723–729.

STEVENS, E. D., RYS, J. & COPPENS, P. (1978). *J. Am. Chem. Soc.* **100**, 2324–2328.

STEWART, R. F. (1976). *Acta Cryst.* A**32**, 565–574.

STROZIER, R. W., CARAMELLA, P. & HOUK, K. N. (1979). *J. Am. Chem. Soc.* **101**, 1340–1343.

SUZUKI, I. (1960). *Bull. Chem. Soc. Jpn*, **33**, 1359–1365.

VOLLAND, W. V., DAVIDSON, E. R. & BORDEN, W. T. (1979). *J. Am. Chem. Soc.* **101**, 533–537.

ZVONKOVA, Z. V., KRIVNOV, V. Y. & KHVATKINA, A. N. (1964). *Dokl. Phys. Chem.* **155**, 261–265.